Shim, Jihye; Lee, Eok Kyun; Lee, Y. -J.; Nieminen, Risto

Density-functional calculations of defect formation energies using supercell methods

Published in:
Physical Review B

DOI:
10.1103/PhysRevB.71.035206

Published: 01/01/2005

Document Version
Publisher's PDF, also known as Version of record

Please cite the original version:
Shim, J., Lee, E. K., Lee, Y. .-J., & Nieminen, R. (2005). Density-functional calculations of defect formation energies using supercell methods: Defects in diamond. *Physical Review B*, *71*(3), 1-12. Article 035206. https://doi.org/10.1103/PhysRevB.71.035206

Density-functional calculations of defect formation energies using supercell methods: Defects in diamond

Jihye Shim and Eok-Kyun Lee
Department of Chemistry and School of Molecular Science (BK21), Korea Advanced Institute of Science and Technology, Taejon, Korea

Y. J. Lee and R. M. Nieminen
Laboratory of Physics, Helsinki University of Technology, P.O. Box 1100, FIN-02015 HUT, Finland
(Received 15 September 2004; revised manuscript received 28 October 2004; published 13 January 2005)

Density-functional theory combined with periodic boundary conditions is used to systematically study the dependence of defect formation energy on supercell size for diamond containing vacancy and self-interstitial defects. We investigate the effect of the electrostatic energy due to the neutralization of charged supercells and the effect of the alignment of the valence band maximum (VBM) on the formation energy. For negatively charged vacancies and positively charged interstitials, the formation energies show a clear dependence on supercell size, and the electrostatic corrections agree with the trend given by the Makov-Payne scheme (Ref. 28). For positively charged vacancies and negatively charged interstitials, the size dependence and the electrostatic corrections are quite weak. An analysis of the spatial charge density distributions reveals that these large variations in electrostatic terms with defect type originate from differences in the screening of the defect-localized charge, as explained by using a simple electron-gas model. Several VBM alignment schemes are also tested. The best agreement between the calculated and asymptotically exact ionization levels is obtained when the levels are based on the formation energies referenced to the VBM of the defect-containing supercell.

DOI: 10.1103/PhysRevB.71.035206 PACS number(s): 71.15.−m, 31.15.Ew

I. INTRODUCTION

Defects in semiconductors not only influence the electrical and optical properties of these materials, but they also exhibit their own interesting physics. The identification and control of defects such as vacancies, interstitials, and impurities is a major field of research, with important applications in materials engineering. Defects have been studied using a wide range of experimental techniques, including electron paramagnetic resonance (EPR) spectroscopy,[1,2] electron-nuclear double resonance (ENDOR) spectroscopy,[3] Hall conductivity,[4,5] positron annihilation,[6,7] and deep-level transient spectroscopy (DLTS).[8,9] These experiments have revealed various types of defects. Moreover, they have shown that the type of defect depends on the history of the material, in particular whether it is natural or synthetic. Defects can exist in several charge states, and various techniques have been developed for identifying the ionization levels which are defined as the Fermi-level (electron chemical potential) positions delineating the stability regions for different charge states.

Defects in semiconductors pose various challenges for theory, including the determination of the origin of experimentally observed defect bands and analyzing the atomic structures of the different charge states.[5] The relative stabilities and concentrations of defects are determined by their formation energies, which primarily depend on the structures and electronic charge states of the defects.[10–13] In addition, the kinetic properties of defects, such as diffusion mechanisms and migration energies, strongly depend on the charge state.[14–16] Moreover, chemical reactions involving bond formation and dissociation can also be explained in terms of the formation energy, provided it can be calculated with sufficient accuracy.[16,17] Systematic formation energy calculations have been performed for several semiconductors, including Si,[18–20] SiC,[21,38] GaN,[22] and diamond.[14,23–25]

The formation energy E_f of a defect with charge q is given by

$$E_f(q) = E_d(q) - N\mu + q(E_V + \mu_e), \tag{1}$$

where $E_d(q)$ is the total energy of the defect-containing system consisting of N atoms, with atomic chemical potential μ. The reservoir of the electrons is described by their chemical potential μ_e, measured relative to the valence band maximum E_V.

The first step in evaluating the formation energy is to calculate the defect energy $E_d(q)$. First-principles density-functional methods have been widely used for this purpose. These methods typically employ periodic boundary conditions (PBC) to mimic the bulk crystal. In fact, PBC are usually applied even in systems lacking three-dimensional periodicity, due to computational advantages. However, real defect-containing systems typically have aperiodic structures and very low defect densities. The elimination of the spurious effects due to the artificial perioidicity is particularly pronounced for systems with charged defects, as they have to be neutralized by adding a fictitious background charge. The slow convergence of the electrostatic energy as a function of the supercell size means that the calculated properties only converge to those of the real system in the limit of an infinitely large supercell. Thus it is important to have a quanti-

tative understanding of the size dependence of the total energy of a given charged system. Several approaches have been developed to solve this problem.

In a mathematical approach to this problem, de Leeuw, Perram, and Smith[26] considered the electrostatic energy of a neutral assembly of classical point charges in a repeated cubic cell. Leslie and Gillan[27] derived the correction term proportional to L^{-1} (L is the linear dimension of the supercell) as the Madelung energy of point charges immersed in a uniform neutralizing background. They applied the correction term to energies of ionic crystals. Makov and Payne[28] generalized the point-charge concept, and developed an additional higher-order correction term depending on L^{-3} and the quadrupole moment M of the defect charge density for cubic supercells. They examined the ionization energies of a Mg atom[28] and several small molecules[29] using supercells and found that the correction improves the result significantly. Kantorovich[30] reexamined the method of Makov and Payne for the case of arbitrary supercell shape, and suggested a new formula ignoring dipole-dipole interactions.

Although the validity of the Makov-Payne correction has been demonstrated for small molecules and several solids, its reliability and generality remain controversial. For instance, for Si with a doubly charged self-interstitial, the linear convergence of the energy difference between the defect-containing and defect-free bulk supercells has been demonstrated, which confirms that the Makov-Payne correction scheme works asymptotically.[31,32] On the other hand, Segev and Wei[33] have recently argued that the electrostatic correction for a defect with shallow electron states is much smaller than that obtained from a localized-charge model. Based on this finding, they argued that no correction is needed for diamond supercells containing more than 128 atoms and an N+4Si defect complex which consists of the N at the T_d site and the four substitutional Si at the corner of tetrahedron. Gerstmann *et al.*[34] calculated the electrostatic energy of V_{Si} in silicon and $V_{\mathrm{Si}}V_{\mathrm{C}}$ in SiC using both Green's function and supercell methods, and compared the ionization levels obtained from the two methods. Surprisingly, they found better agreement between these methods when the Makov-Payne correction was not applied.

Schultz developed a method based on the local-moment countercharge (LMCC) concept, which also assumes that the charge is localized.[35,36] Under this approach, the charge distribution is considered to have a finite range and proper electrostatic moments. The electrostatic energy is calculated separately, assuming that the remaining part of the system is a defect-free, perfect nonpolarizable bulk crystal. This method explicitly takes into account that the defect charge has a finite distribution. However, the electronic response of the bulk region is not considered, and unfortunately, no analytical correction formula is available for this method.

Another important physical parameter for the calculation of the formation energy is the position of the valence band maximum (VBM) E_V, which corresponds to the reference energy level for the electron chemical potential. The position of the VBM of the defect-containing supercell is different from that of the defect-free bulk supercell, and the magnitude of this difference depends on the charge state. Several methods have been suggested to align the VBM of a defect. One of the most frequently used methods is to correct the VBM of the bulk supercell by an average potential difference,[37] which shifts it by an amount equal to the difference in the average effective potential, $\overline{V}_{\mathrm{bulk}}-\overline{V}_d$ between bulk and defect-containing supercells.[13] Another suggestion is to use the lowest energy level as a reference.[38]

An alternative way to determine the ionization level that avoids the VBM problem is the marker method.[39] This method compares the ionization energies with reference defect-containing systems whose electrical levels are known from experiment. The marker method works best when the ionization level of the unknown defect is close to one of the markers. Alternatively, *ab initio* data obtained from a bulk supercell of the same size can also be used as markers.[40] For more details, see Ref. 41 and the references therein.

To summarize, there are two ambiguous points in the calculation of the formation energies within the supercell framework. First, the electrostatic correction due to the charge neutralization has not been examined systematically. Second, there is no generally accepted scheme to determine or align the VBM, despite numerous schemes having been proposed. In the present work we have carried out a systematic investigation of the effect of supercell size on calculated formation energies. We use the vacancy and self-interstitial defects in diamond as the test case. As a wide-band gap material, diamond supports several charge states in its native defects. In addition, these have widely different distributions of localized charge, which enables a systematic study of the finite-supercell-size effects. The structure of this paper is as follows. First we provide a brief description of the computational methods and present the defect electronic structures (Sec. II and Sec. III A). In Sec. III B, we investigate the convergence of the calculated total energies as a function of supercell size, and the link between electrostatic correction and defect type. In Sec. III C, several VBM schemes are described and discussed. In Sec. III D, we discuss in detail the effect of electrostatic energy and VBM scheme on the relative stabilities and ionization levels of various charge states. A brief summary and our conclusions are given in Sec. IV.

II. COMPUTATIONAL METHODS

The calculations were performed using density-functional theory (DFT) within the spin-polarized generalized-gradient approximation (sp-GGA), with the functional of Perdew, Burke, and Ernzerhof (PBE)[42] for the exchange correlation energy. Only valence electrons were considered using numerical atomic basis functions, and their interactions with core electrons were treated by norm-conserving scalar-relativistic pseudopotentials including nonlinear partial-core corrections. These are implemented in the fully self-consistent *ab initio* package SIESTA, which has been used.[43]

We use double-ζ basis functions for s and p orbitals, and a single polarization function for d orbitals. The orbital ranges are $r_c=4.63$ and 3.43 for s, $r_c=5.66$ and 3.65 for p, and $r_c=5.66$ Bohr for d orbitals. The real-space mesh grid is determined by the maximum kinetic energy of the plane-wave, which is 100 Ry. The electronic iterations were con-

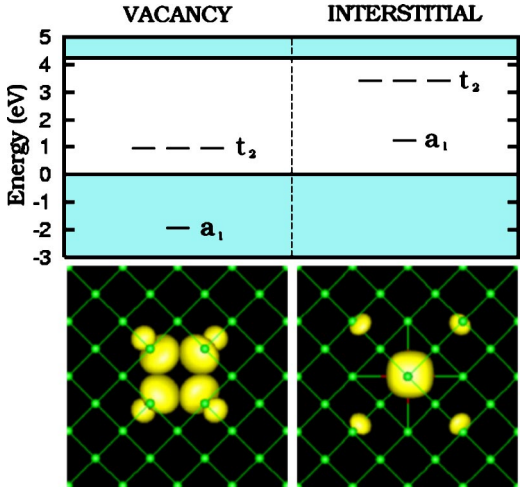

FIG. 1. (Color online) [Top] Schematic diagram of the calculated Kohn-Sham levels at Γ point for a vacancy (left) and interstitial (right) in a neutral charge state in the 432-atom supercell. [Bottom] Constant-electron-density surfaces, drawn for the t_2 levels at 10% of the maximum density.

tinued until the total energy difference relative to the previous step was smaller than 10^{-5} eV. The convergence of **k**-point sampling was tested for a two-atom bulk unit cell with an increasing number of sampling points using the Monkhorst-Pack (MP) scheme, and full convergence was obtained at a $7\times7\times7$ MP **k**-point mesh. The calculated lattice constant and band gap are 3.59 Å and 4.2 eV, respectively. The corresponding experimental values are 3.57 Å and 5.49 eV. We use the lattice constant of 3.59 Å in all of our calculations. For Brillouin-zone sampling, uniform MP meshes of 3^3, 3^3, 2^3, 2^3, and 1^3 were used for the 32-, 64-, 128-, 216-, and 432-atom supercells, respectively, which are equivalent to the **k**-point sampling with a 7^3 MP mesh for the two-atom supercell.

III. RESULTS AND DISCUSSION

A. Electronic Structure

As prototypical defects, we consider the monovacancy and the T_d interstitial in diamond, which have various charge states in the wide band gap. Schematic diagrams of the one-electron energy levels and localized electron densities of the vacancy and interstitial defects are shown in Fig. 1. For the neutral vacancy and interstitial, four electrons must be placed in the localized defect states: two in the a_1 state and two in the t_2 state, giving the configuration $a_1^2t_2^2$. With this configuration, we investigate all the possible charge states ranging from +2 to −4.

B. Total Energy Convergence

To investigate the effect of supercell size on the total energy, we define the energy term independent of the VBM position,

$$E_{\mathrm{def}}(L,q) = E_d(L,q) - N\mu, \tag{2}$$

where $E_d(L,q)$ is the total energy of the defect-containing supercell with charge q, L is the cubic root of the supercell volume, and μ is the atomic chemical potential, corresponding to the defect-free supercell energy per atom. We calculate $E_{\mathrm{def}}(L,q)$ for the seven charge states (+2, +1, 0, −1, −2, −3, and −4) for the vacancy and T_d-interstitial defects. All the calculations are performed without atomic relaxation in order to focus on only the electrostatic energy terms.

All the calculated values of $E_{\mathrm{def}}(L,q)$, except that calculated for the smallest supercell (32 atoms), are well fitted by a straight line (dashed) for all the charge states considered, as shown in Fig. 2. The differences between the filled triangle at each L and the solid horizontal line (the asymptotic value) are considered as the electrostatic correction energies. For the 432-atom supercell they are −0.05, 1.04, 0.80, and 0.03 eV for V^{+2}, V^{-2}, I^{+2}, and I^{-2}, respectively. The $E_{\mathrm{def}}(L,q)$ values and their extrapolated values for all the charge states are given in Table I and plotted in Fig. 2 for $q=\pm2$. For the vacancy defect, the electrostatic correction is quite large for the negative charge state [Fig. 2(b)] but small for the positive charge state [Fig. 2(a)]. In contrast, for the interstitial defect it is large for the positive charge state [Fig. 2(c)] but close to zero for the negative charge state [Fig. 2(d)]. It is interesting that two systems with the same type of defect but opposite charge states show totally different behavior.

The Makov-Payne scheme[28] for the electrostatic correction is as follows:

$$E_{\mathrm{def}}^{\mathrm{MP}}(L,q) = E_{\mathrm{def}}(L,q) + \frac{q^2\alpha}{2L\epsilon} + \frac{2\pi qM}{3L^3\epsilon} + O(L^{-5}), \tag{3}$$

where ϵ is the dielectric constant (we use below the experimental value of 5.5), and α is the Madelung constant (2.8373, 2.8883, and 2.885 for a simple cubic, body-centered cubic, and face-centered cubic supercell, respectively).[27] As the L^{-3}-dependency is not clear, as can be seen in Fig. 2, we only consider the linear L^{-1} term. The validity of the Makov-Payne scheme can be examined by comparing the result before and after applying the scheme (i.e., compare the filled triangles with the empty diamonds in Fig. 2). For vacancy defects in a negative charge state and interstitial defects in a positive charge state, the correction describes well the electrostatic energy due to charge neutralization. For vacancies in a positive charge state and interstitials in a negative charge state, in contrast, the Makov-Payne scheme significantly overestimates the correction. For the 432-atom supercell, the overestimations of the correction compared to the exact asymptotic value are 0.08, 0.31, 1.16, and 1.08 eV for V^{-2}, I^{+2}, V^{+2}, and I^{-2}, respectively.

Two questions now arise: (1) Why do defects of the same type but in opposite charge states exhibit totally different variations in the electrostatic energy with changing supercell size? (2) Why is this trend reversed on going from vacancy to interstitial?

To understand the origin of the electrostatic energy terms outlined above, we investigate the charge density, $\Delta\rho_q(\vec{r})$,

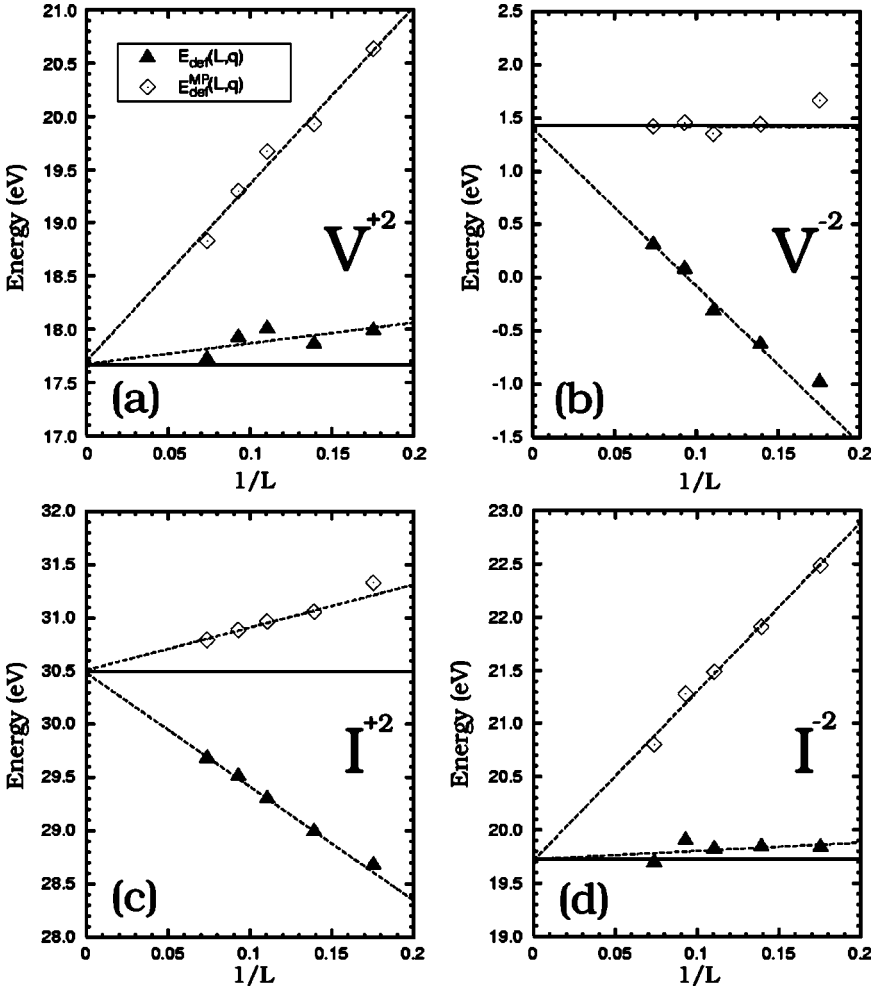

FIG. 2. $E_{\mathrm{def}}(L,q)$ for the 32-, 64-, 128-, 216-, and 432-atom supercells (filled triangles) and the corrected energies using the Makov-Payne scheme $E_{\mathrm{def}}^{\mathrm{MP}}(L,q)$ (empty diamonds). Horizontal solid lines are the extrapolated values of $E_{\mathrm{def}}(L,q)$ at $1/L=0$ of linear fits (dashed lines) to the data (symbols). The total energies are calculated without supercell relaxation. (a) V^{+2}, (b) V^{-2}, (c) I^{+2}, and (d) I^{-2}.

which is the sum of the electron density difference between the charged and neutral systems and the uniform background (neutralization) density. In our notation, the electron density is always positive. Here we present the calculation results for $q=\pm 2$, which are representative of the results obtained for the other charge states. The calculated radial charge distributions show the highest peak near the defect, immediately followed by a strong peak of opposite sign, as shown in Fig. 3. This indicates that the charge density is strongly localized around the defect, as expected from Fig. 1, and that the defect is screened by the electrons in the surrounding bulk. The differences in screening among the various charge states are clearly seen from the integrated charge density, $Q(r)$, in Figs. 3(c) and 3(d). Near the first atomic shell, the $Q(r)$ of V^{-2} is almost twice that of V^{+2}. For the interstitial, the $Q(r)$ of I^{-2} is smaller than that of I^{+2} by almost one third over the entire range of r. The lower values of $Q(r)$ for V^{+2} and I^{-2} mean that the localized charges are more efficiently screened. Conversely, the higher values of $Q(r)$ for V^{-2} and I^{+2} imply that the localized charges are less efficiently screened.

The screening electrons result from the response of the outer electrons in the bulk region because the electrons at the defect levels are strongly localized, as shown in Fig. 1. We investigate the response of the valence electrons in the bulk by dividing the total charge density $[\Delta\rho_q(\vec{r})]$ into the defect charge $[\Delta\rho_q^d(\vec{r})]$ and the valence charge $[\Delta\rho_q^v(\vec{r})]$, defined as follows:

$$\Delta\rho_q^v(\vec{r}) = \sum_{i=1}^{\mathrm{VBM}} |\psi_q^i(\vec{r})|^2 - \sum_{i=1}^{\mathrm{VBM}} |\psi_0^i(\vec{r})|^2 + n_0 \tag{4}$$

$$\Delta\rho_q^d(\vec{r}) = \sum_{i>\mathrm{VBM}}^{occ} |\psi_q^i(\vec{r})|^2 - \sum_{i>\mathrm{VBM}}^{occ} |\psi_0^i(\vec{r})|^2, \tag{5}$$

where $|\psi_q^i(\vec{r})|^2$, the electron density at $\vec{r}$ of ith band is averaged for given $\mathbf{k}$ points, and n_0 is the uniform background charge. We consider only the t_2 level for the defect charge because the a_1 level is below the VBM.

Figure 4 shows that the defect charges (solid line) and valence charges (dashed line) of V^{+2} and I^{-2} are localized with similar shape but opposite sign within the range of $r=2$ Å (i.e., of the order of one atomic radius), indicating that the defect charges are effectively compensated. In the bulk region, small resonance peaks of the defect and valence charges give rise to oscillations in the charge density, as seen in Fig. 3. For a graphical view, the defect and valence charges for the cases of V^{+2} and I^{-2} are depicted as two-dimensional contour plots in Fig. 5. From this investigation, the localized charge in Fig. 3 can be explained as the defect

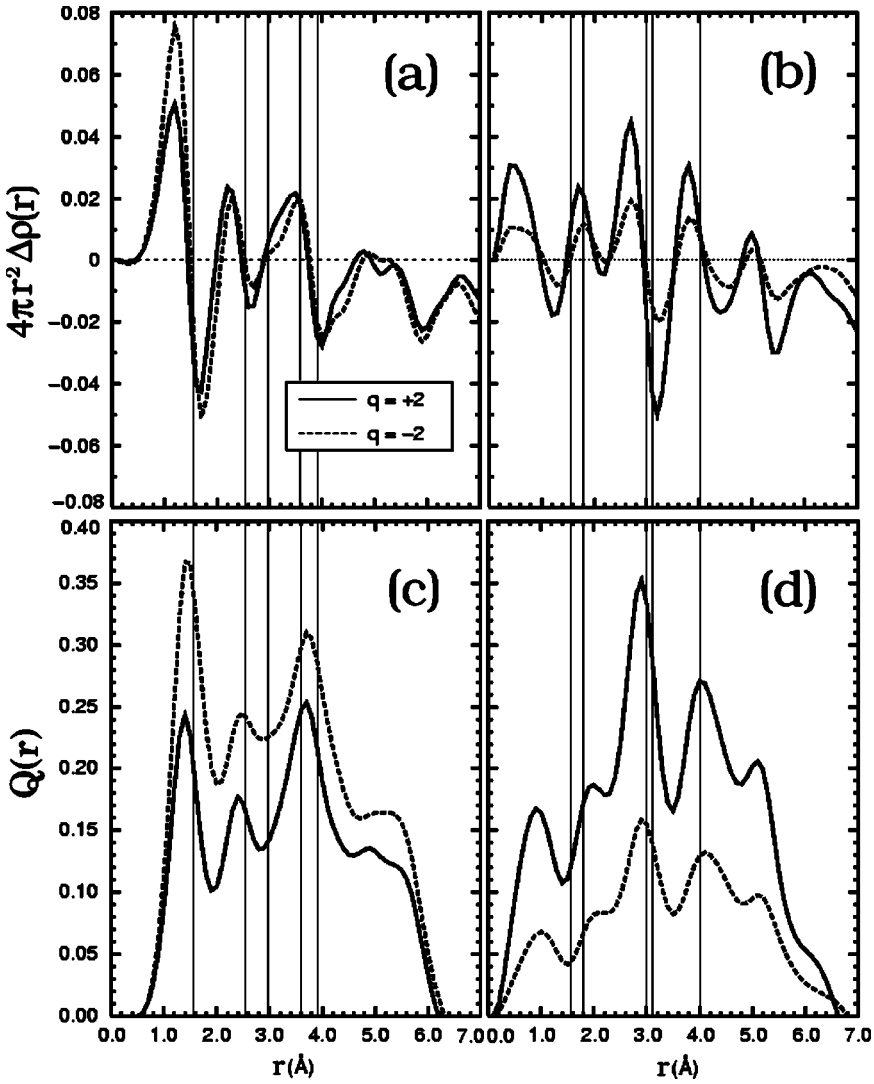

FIG. 3. The calculated radial distributions $4\pi r^2 \Delta\rho_q(r)$ [(a) and (b)] and their integrated charges $Q(r) = \int_0^r 4\pi r'^2 \Delta\rho_q(r')dr'$ [(c) and (d)] for 216-atom supercells: (Ref. 44) (a) and (c) vacancies; and (b) and (d) interstitials. Solid and dashed lines are for +2 and −2 charge states, respectively. For convenience, the numerical values of the charge densities for V^{+2} and I^{+2} are multiplied by −1. Vertical lines indicate the locations of the neighboring atom shells.

charge screened by the valence charge near the defect. Similarly, the screening charge is the remaining longer-ranged valence charge. A strong screening by bulk valence electrons explains a small electrostatic correction.

To understand why positively charged vacancies and negatively charged interstitials are characterized by a greater degree of screening than negative vacancies and positive interstitials, we consider a simple electron gas model. In this model, the defect-free perfect supercell is approximated as a box with uniform electron density. On the other hand, the supercell containing a vacancy defect is modeled as a region of uniform electron density with an electron-deficient cavity [Fig. 6(a)], and the supercell containing an interstitial defect is modeled as a region of uniform electron density with a protrusion of excess electrons [Fig. 6(d)]. In these defect models, the electrons in the bulk will respond so as to remove the perturbation induced by the defect (cavity or protrusion), resulting in flow in to the cavity [Fig. 6(a)] or flow out from the protrusion [Fig. 6(d)]. If the charging is in a direction that reinforces the existing perturbation, the electrons in the bulk region will strongly respond to remove the additional perturbation induced by the charging, resulting in a weak electrostatic interaction. If, however, the charging offsets an existing perturbation, the bulk electrons will respond weakly, resulting in a strong electrostatic interaction.

One quantitative measure for the response of electrons in the valence band is the Mulliken population obtained from atomistic calculations. For the case of a vacancy in diamond, the Mulliken populations of the neighboring atoms (calculated using a 432-atom supercell) are 4.059, 4.028, and 4.116 for V^0, V^{-2}, and V^{+2}, respectively, indicating that 0.06, 0.03, and 0.12 excess electrons are transferred from the bulk region towards the vacancy (cavity). For the case of an interstitial, on the other hand, the Mulliken populations of the interstitial atom are 3.528, 3.471, and 3.547 for I^0, I^{-2}, and I^{+2}, respectively, indicating a transfer of 0.47, 0.53, and 0.45 valence electrons near the defect (protrusion) toward the bulk region. For both defect systems, the order of charge transfer (valence electron response) is in perfect agreement with the magnitude of the perturbation. Thus the simple free electron

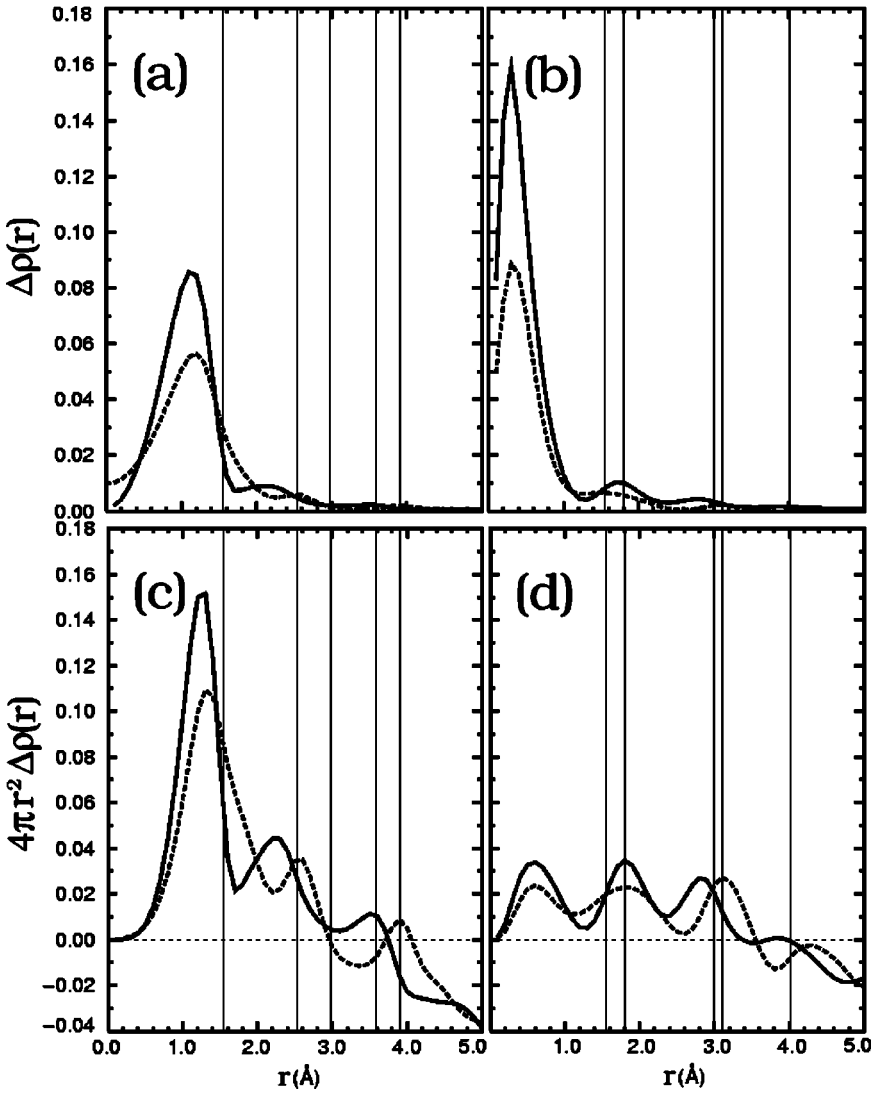

FIG. 4. The average radial distributions of the defect (bold line) and valence (dashed line) charges for (a) V^{+2} and (b) I^{-2} of the 216-atom supercell. The radial distributions are also presented for (c) V^{+2} and (d) I^{-2}. To facilitate comparison, the valence charge of V^{+2} and the defect charge of I^{-2} are multiplied by −1.

gas model discussed above is consistent with the atomistic results and qualitatively explains the magnitude of the electrostatic energy correction.

C. Valence Band Maximum

According to Eq. (1), the formation energy of a charged defect depends on the chemical potential μ_e measured relative to the electron reference level E_V. However, the VBM of a defect-containing supercell is different from that of a bulk supercell of the same size. Moreover, if the supercell contains a defect, the VBM depends on the size of the supercell. For example, the differences between the VBMs of the neutral vacancy containing and bulk supercells are 0.66, 0.21, and 0.07 eV for the 64-, 128-, and 432-atom supercells, respectively; this dependence on the supercell size can cause significant problems in the estimation of the formation energy as well as the ionization levels.

The formation energies calculated using three different VBMs are presented in Fig. 7. First, the VBM of the bulk supercell (*bulk* VBM) is used for all the charge states. Second, we consider the *bulk* VBM with the average potential correction for each system, where the average is taken over mesh points lying inside a sphere with the radius of half a bond length on the sites furthest away from the defect site. The average potential differences are calculated at the position of the atom, the midpoint of the bond, and the interstitial position. The correction values are not more than a few tens of million electron volts throughout the positions in the region far from the defect site. The third scheme is using the VBM of the defect-containing supercell (*defect* VBM), where the *defect* VBM is determined by the band structure calculation of the corresponding supercell.

Three notable points concerning the VBM schemes can be discerned in Fig. 7. First, for supercells containing more than 128 atoms, the dependence of the formation energy on the VBM scheme is negligible compared to the magnitude of the electrostatic correction discussed above. Second, the average potential correction to the *bulk* VBM changes the formation energy only slightly. Third, the application of the *defect* VBM instead of the *bulk* VBM results in somewhat incon-

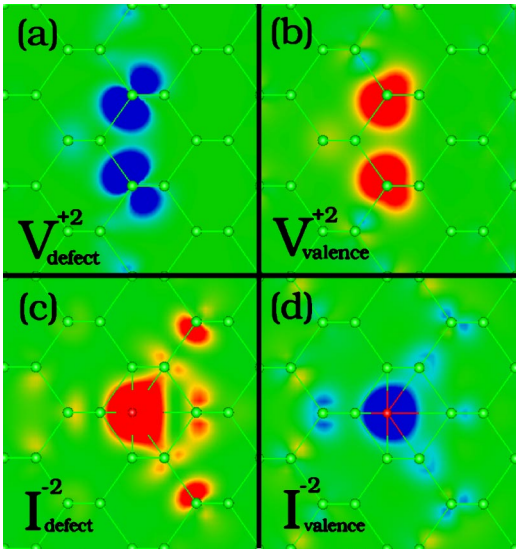

FIG. 5. (Color online) Two-dimensional plot of the charge density of defects in the 216-atom supercell. The defect charge and the valence charge are plotted separately as follows: (a) defect charge of V^{+2}, (b) valence charge of V^{+2}, (c) defect charge of I^{-2}, and (d) valence charge of I^{-2}. The color scale is from −0.005 to 0.005 electrons/Å^3. The minimum and maximum values are encoded as blue and red, respectively.

sistent behavior; for V^{-2}, for example, the use of *defect* VBM rather than *bulk* VBM gives better results. The VBM methods will be discussed in further detail in the next section, where we discuss the ionization levels.

D. Thermodynamically Stable Charge States and Ionization Levels

We now investigate the effect of the supercell size on the thermodynamic stability of charge states and the ionization levels. The total energies are calculated for *unrelaxed* supercells, in order to concentrate exclusively on the effect of supercell size.

The *computationally exact* formation energy of a defect, within the DFT scheme, can be calculated from the exact $E_{\mathrm{def}}(L,q)$ and E_V. The exact $E_{\mathrm{def}}(L,q)$ is obtained by extrapolating the data for the finite supercells to $L\rightarrow\infty$, and the exact E_V is equal to that of the defect-free bulk supercell. The exact formation energy can thus be expressed as

$$E_f^{\mathrm{ext}}(L,q) = E_{\mathrm{def}}^{\mathrm{ext}}(L,q) + q(E_V^{\mathrm{bulk}} + \mu_e). \tag{6}$$

We compare the formation energy diagrams of the 128- and 432-atom supercells with that constructed using the exact values. Since we have already confirmed that the VBM scheme has a negligible effect on the formation energy for sufficiently large supercells, we use the *bulk* VBM for both the 128- and 432-atom supercells. First, let us consider the results for the case of a vacancy in diamond. Figure 8(a) presents the diagram of exact vacancy formation energies for different charge states. This diagram shows that, as the electron chemical potential increases, the thermodynamically

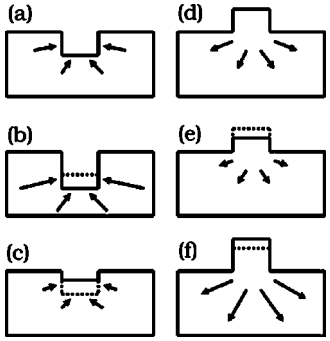

FIG. 6. A schematic representation of the electron gas model. (a) V^0, (b) V^{+2}, (c) V^{-2}, (d) I^0, (e) I^{+2}, and (f) I^{-2}.

stable electronic charge state of a vacancy changes from a doubly positive state to a neutral state, and then to a negative state. The negative-U phenomenon is seen to exclude the singly positive charge state. Near the conduction band edge, the transition from a singly negative to a doubly negative $(-/2-)$ state is observed, but the exact energy position of this transition is not available due to the fact that standard DFT underestimates the band gap. (The calculated band gap is 1 eV smaller than the experimental value for diamond.) For the 128-atom supercell [Fig. 8(c)], the negative-U effect disappears and the $(2+/+)$ level shifts toward the valence band by 0.8 eV. In the case of negative charge states, the energy levels become deeper and a stable V^{-2} state appears. When the Makov-Payne correction is applied [Fig. 8(b)], the vacancy no longer stabilizes the +2 and −2 charge states, and the stability of the neutral state is enhanced. For the 432-atom supercell, which is generally believed to be large enough for accurate calculation, the positive levels are very close to the exact values whereas the negative levels still differ from the exact values by more than 0.5 eV [Fig. 8(d)].

Next, we examine the formation energy diagrams of interstitials. As shown in Fig. 8(e), the route along which the stable electronic charge state varies is as follows. Starting from the doubly positive state, with increasing μ_e the system shifts to a singly positive state, then to the neutral state, and finally ends up in a singly negative state. In addition, Fig. 8(e) reveals that the order of the stable charge states is the same for the 128- and 432-atom supercells. Since the positive state $(2+/+)$ is located at midgap, it is likely that the stability of the state will not be much affected by either supercell size or electrostatic energy correction. For the 128-atom supercell, this level becomes deeper than the exact value by about 0.6 eV, while it becomes shallower by almost the same amount after the Makov-Payne correction. For the 432-atom supercell, this level is still deeper than the exact value by about 0.4 eV. The levels for the negative charge states are barely affected by the supercell size, shown in Table. I. The question still remains, however, as to whether the doubly negative charge state is in fact a stable state, since it is located just below the Kohn-Sham band edge.

Tables II and III list the specific ionization levels for the various supercell sizes, the electrostatic correction, and the VBM alignment scheme for vacancies and interstitials, respectively. The ionization levels between thermodynamically

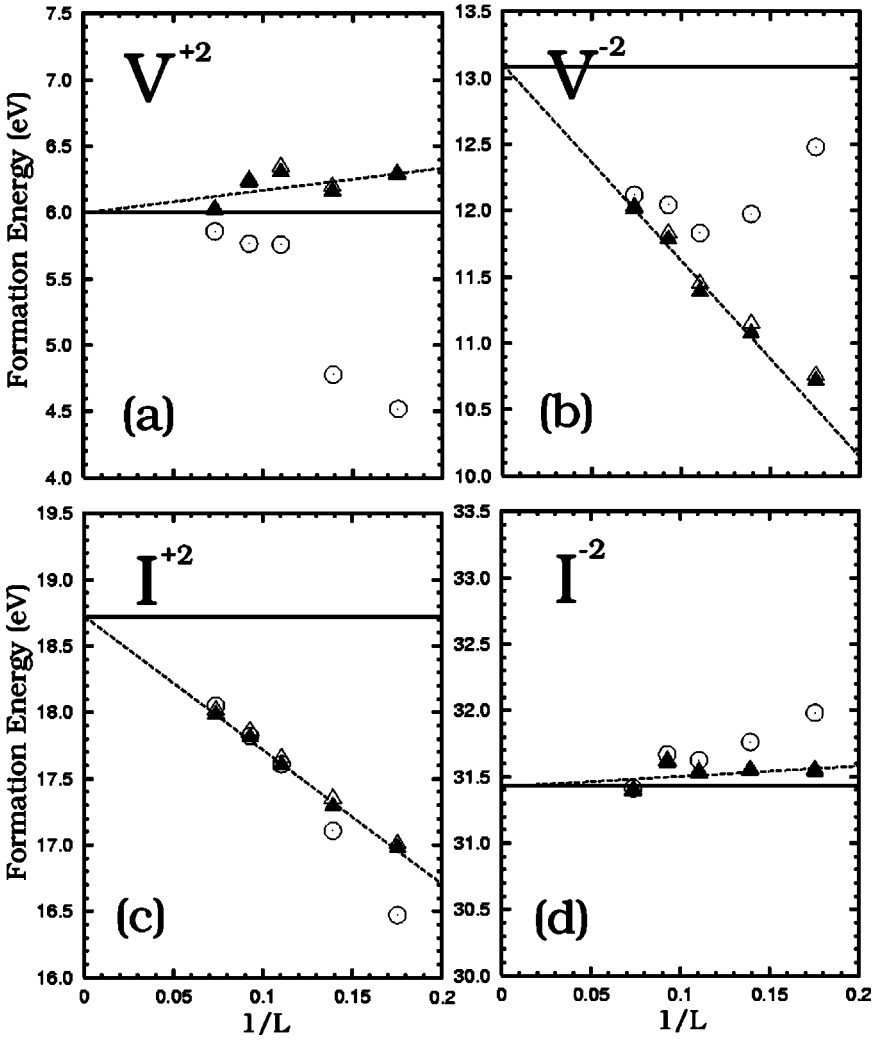

FIG. 7. Formation energies as a function of $1/L$, calculated using *bulk* VBM (filled triangles), *bulk* VBM corrected by the average potential difference (empty triangles), and *defect* VBM (circles). Dashed lines indicate linear fits to the *bulk*-VBM data, and the solid horizontal line is the value extrapolated to $1/L=0$.

stable states within the calculated band gap are shown in boldface. Where unphysical negative ionization levels were obtained, the result is shown as a dash. In the last column, the aggregate standard deviation of ionization level positions from the computationally exact values S_N is given as

$$S_N = \sqrt{\frac{1}{N_l}\sum_{i=1}^{N_l}(x_i^N - x_i^{\mathrm{ext}})^2}, \tag{7}$$

where x_i^N is the ith ionization level of an N-atom supercell, x_i^{ext} is the extrapolated value of the ith ionization level, and N_l is the number of ionization levels. The magnitude of S_N can be used as a quantitative measure of the overall accuracy with which each computational scheme pinpoints the ionization levels. A smaller S_N implies a more reliable overall scheme, but does not of course guarantee that every ionization level is more accurate.

As expected, for each scheme S_N decreases with increasing supercell size. Notably, for the vacancy defect, the smallest S_N is obtained when the *defect* VBM is used. For the interstitial defect, the average potential correction method shows the smallest S_N, and the *defect* VBM also gives good results. The Makov-Payne correction increases S_N for both the *bulk* VBM and *defect* VBM schemes. Especially for the interstitial case, the values obtained without the Makov-Payne correction are about five times smaller than those obtained with this correction. If one wants to estimate the relative stabilities of various charge states without any prior knowledge about the system, the use of the *defect* VBM without electrostatic energy correction usually gives the most reliable results.

IV. CONCLUSIONS

We have studied the dependence of defect formation energies on supercell size for charged vacancy and interstitial defects in diamond. Our study is focused on the electrostatic energy and on the alignment of the valence band maximum.

The electrostatic correction for charged systems is often estimated using the Makov-Payne scheme, within which the electrostatic energy is proportional to the square of the charge on the defect, assuming that the defect charge is

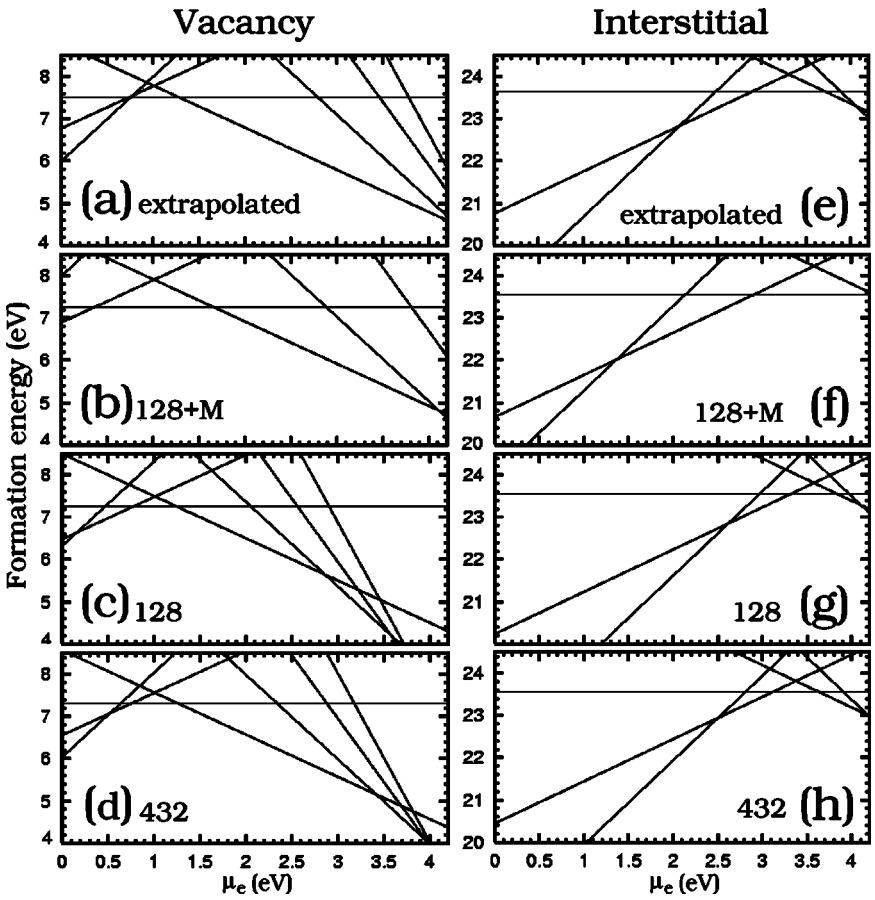

FIG. 8. Formation energies for the various charge states for the *unrelaxed* vacancy and interstitial in diamond as a function of the electron chemical potential. They are calculated from (a), (e) the extrapolated values, (b), (f) 128-atom supercell data with the Makov-Payne correction, (c), (g) 128-atom supercell data without the Makov-Payne correction, and (d), (h) 432-atom supercell data without the Makov-Payne correction. For all the cases, the *bulk* VBM is applied.

TABLE I. $E_{\mathrm{def}}(L,q)$ of various supercells and their values when extrapolated to $L\rightarrow\infty$. All values are in electron volts.

q	32	64	128	216	432	ext
			Vacancy			
+2	17.98	17.85	18.03	17.92	17.72	17.67
+1	12.42	12.29	12.32	12.50	12.38	12.59
0	7.16	7.20	7.26	7.38	7.31	7.51
−1	2.47	2.55	2.66	2.71	2.73	2.95
−2	−0.98	−0.63	−0.31	0.08	0.37	1.49
−3	−4.30	−3.31	−2.58	−2.14	−1.56	0.35
−4	−7.05	−5.65	−4.48	−4.06	−3.28	−0.69
			Interstitial			
+2	28.68	28.99	29.30	29.51	29.68	30.35
+1	25.87	26.00	26.08	26.29	26.28	26.59
0	23.52	23.58	23.55	23.67	23.54	23.65
−1	21.43	21.54	21.55	21.58	21.35	21.52
−2	19.83	19.84	19.82	19.90	19.69	19.74
−3	18.50	18.48	18.30	18.27	18.03	17.92
−4	17.15	17.28	17.00	17.09	16.50	16.48

TABLE II. The ionization levels for the *unrelaxed* supercells containing a vacancy defect. S_N is the aggregate standard deviation from the exact ionization levels calculated from the extrapolated formation energies. All values are in electron volts.

	(+2/+)	(+2/0)	(+/0)	(0/−)	(−/2−)	(0/2−)	(2−/3−)	(0/3−)	(3−/4−)	(0/4−)	S_N
					Defect VBM						
32	**0.906**	1.093	**1.280**	**1.883**	**3.269**	2.576	**3.609**	2.920	**4.015**	3.194	0.670
64	**1.092**	1.171	**1.249**	**1.587**	**3.113**	2.350	**3.653**	2.784	**4.014**	3.092	0.708
128	**0.525**	0.757	**0.990**	**1.441**	**3.098**	2.270	**3.816**	2.785	**4.166**	3.130	0.640
216	**0.746**	0.808	**0.870**	**1.287**	**3.359**	2.323	**3.755**	2.800	**4.038**	3.110	0.602
432	**0.636**	0.727	**0.818**	**1.326**	**3.468**	2.397	**3.978**	2.924	**4.079**	3.213	0.513
					Defect VBM and Makov-Payne correction						
32	—	—	**0.0617**	**2.546**	5.258	3.902	6.926	4.910	8.658	5.847	1.876
64	—	0.136	**0.732**	**2.105**	4.665	3.385	6.239	4.336	7.634	5.161	1.302
128	—	—	**0.572**	**1.859**	**4.350**	3.104	5.902	4.037	7.087	4.799	1.106
216	—	0.118	**0.525**	**1.632**	**4.394**	3.013	5.479	3.835	6.452	4.489	0.804
432	—	0.170	**0.540**	**1.604**	**4.302**	2.953	5.369	3.758	6.027	4.326	0.664
					Bulk VBM						
32	**0.287**	0.438	**0.590**	**1.155**	**2.400**	1.777	**2.533**	2.029	**3.103**	2.298	1.311
64	**0.280**	0.520	**0.760**	**1.206**	**2.667**	1.937	**3.168**	2.347	**3.507**	2.637	1.026
128	**0.168**	0.478	**0.787**	**1.256**	**2.871**	2.064	**3.590**	2.573	**3.948**	2.916	0.820
216	**0.436**	0.580	**0.725**	**1.170**	**3.229**	2.200	**3.643**	2.681	**3.932**	2.994	0.703
432	**0.530**	0.647	**0.764**	**1.272**	**3.428**	2.350	**3.975**	2.892	**0.084**	3.190	0.534
					Bulk VBM corrected by average potential difference						
32	**0.278**	0.434	**0.591**	**1.169**	**2.426**	1.797	**2.568**	2.054	**3.148**	2.328	1.288
64	**0.251**	0.502	**0.753**	**1.225**	**2.722**	1.974	**3.256**	2.401	**3.621**	2.706	0.975
128	**0.136**	0.457	**0.777**	**1.272**	**2.915**	2.094	**3.662**	2.617	**4.020**	2.967	0.786
216	**0.419**	0.569	**0.720**	**1.182**	**3.263**	2.223	**3.696**	2.714	**3.985**	3.032	0.674
432	**0.524**	0.643	**0.762**	**0.277**	**3.441**	2.359	**3.990**	2.903	**4.103**	3.203	0.525
					Bulk VBM and Makov-Payne correction						
32	—	—	—	**1.818**	**4.390**	3.104	5.849	4.019	7.746	4.951	1.523
64	—	—	**0.243**	**1.724**	**4.219**	2.971	5.755	3.899	7.128	4.706	1.229
128	—	—	**0.370**	**1.674**	**4.123**	2.898	5.677	3.824	6.869	4.585	1.098
216	—	—	**3.380**	**1.515**	**4.263**	2.889	5.367	3.715	6.346	4.373	0.833
432	—	0.090	**0.486**	**1.550**	**4.263**	2.907	5.366	3.727	6.032	4.303	0.686
Ext	0.803	0.771	**0.739**	**1.283**	**4.305**	2.794	4.807	3.465	4.738	3.783	

pointlike localized at the defect. This scheme does not account for the polarization of and screening by the valence electrons. For isolated ions or molecules surrounded by vacuum, the electrostatic energy is accurately described by the Makov-Payne scheme,[28] because the surrounding vacuum does not require any extra considerations of polarizability and screening. However, in the case of a defect in a solid, the bulk valence electrons respond to and screen the localized defect charge, and hence the effective charge is less than the nominal charge.

The present analysis based on the radial charge distribution clearly shows that the degree of screening of the localized charge by the bulk valence electrons depends on the charge state and defect type, and consequently plays a critical role in determining the electrostatic interaction energy. A qualitative explanation for the role of screening is obtained by considering the Mulliken population data from atomistic calculations using a simple electron gas model. When the electron density of the defect system is perturbed more strongly by charging (positively charged vacancies or negatively charged interstitials), the defect charge is screened to a greater extent by the valence electrons, and hence the remaining electrostatic interactions become weaker. In this case, the energy correction by the Makov-Payne scheme gives unreasonable results. In contrast, if the charging compensates for an existing perturbation (negatively charged vacancies or positively charged interstitials), the large electrostatic energy is well described by the Makov-Payne scheme. The trends observed for the electrostatic corrections for supercell calculations of silicon vacancies and interstitials are also consistent with those for diamond, and can be explained by our qualitative model.[45]

TABLE III. The ionization levels for the *unrelaxed* supercells containing an interstitial defect. S_N is the aggregate standard deviation from the exact ionization levels calculated from the extrapolated formation energies. All values are in electron volts.

	(+2/+)	(+2/0)	(+/0)	(0/−)	(−/2−)	(0/2−)	(2−/3−)	(0/3−)	(3−/4−)	(0/4−)	S_N
						Defect VBM					
32	**3.288**	3.526	**3.764**	**3.980**	4.479	**4.229**	4.798	4.419	4.894	4.538	0.705
64	**2.939**	3.237	**3.536**	**3.916**	4.264	**4.090**	4.619	**4.266**	4.862	4.415	0.515
128	**2.592**	2.969	**3.345**	**3.908**	4.172	**4.040**	4.395	**4.158**	4.653	**4.282**	0.328
216	**2.607**	2.926	**3.245**	**3.792**	4.203	**3.998**	4.260	**4.085**	4.740	**4.249**	0.294
432	**2.452**	2.780	**3.108**	**3.666**	4.207	**3.936**	4.202	**4.025**	4.353	**4.107**	0.166
						Defect VBM and Makov-Payne correction					
32	**1.298**	2.199	**3.101**	4.643	6.469	5.556	8.114	6.409	9.537	7.191	2.647
64	**1.387**	2.203	**3.018**	4.433	5.816	5.125	7.205	5.818	8.483	6.484	2.063
128	**1.340**	2.134	**2.928**	**4.325**	5.423	4.874	6.481	5.410	7.574	5.951	1.618
216	**1.573**	2.236	**2.900**	**4.137**	5.237	4.687	5.984	5.119	7.154	5.628	1.348
432	**1.617**	2.224	**2.830**	**3.944**	5.042	4.493	5.593	4.860	6.301	5.220	1.013
						Bulk VBM					
32	**3.030**	3.263	**3.497**	**3.749**	**4.241**	3.995	4.502	4.164	4.498	4.247	0.473
64	**2.848**	3.135	**3.423**	**3.797**	**4.143**	3.970	4.476	4.139	4.641	4.264	0.407
128	**2.617**	2.963	**3.309**	**3.848**	**4.106**	3.977	4.324	4.093	4.535	4.203	0.295
216	**2.625**	2.922	**3.219**	**3.750**	**4.156**	3.953	**4.211**	4.039	4.656	4.194	0.272
432	**2.504**	2.805	**3.106**	**3.645**	4.184	3.914	**4.176**	4.001	4.317	4.080	0.174
						Bulk VBM corrected by average potential difference					
32	**3.008**	3.248	**3.489**	**3.754**	**4.254**	4.004	4.520	4.176	4.514	4.260	0.470
64	**2.808**	3.105	**3.403**	**3.798**	**4.154**	3.976	4.494	4.149	4.663	4.277	0.398
128	**2.576**	2.935	**3.294**	**3.854**	**4.120**	3.987	4.334	4.103	4.549	4.214	0.285
216	**2.588**	2.897	**3.206**	**3.759**	**4.167**	3.963	4.224	4.050	4.663	4.204	0.262
432	**2.409**	2.753	**3.097**	**3.650**	4.189	3.919	4.181	4.006	4.330	4.087	0.166
						Bulk VBM and Makov-Payne correction					
32	**1.040**	1.937	**2.833**	**4.412**	6.231	5.322	7.818	6.154	9.141	6.900	2.432
64	**1.296**	2.101	**2.906**	**4.314**	5.694	5.004	7.062	5.690	8.262	6.333	1.948
128	**1.366**	2.129	**2.891**	**4.265**	5.357	4.811	6.411	5.344	7.456	5.872	1.555
216	**1.591**	2.232	**2.874**	**4.095**	5.191	4.643	5.935	5.074	7.070	5.573	1.304
432	**1.669**	2.248	**2.827**	**3.923**	5.019	4.471	5.567	4.836	6.265	5.193	0.990
Ext	**2.081**	2.490	**2.899**	**3.713**	4.061	3.887	**4.018**	3.931	4.399	4.048	

We have also studied the method of VBM alignment with a view to more accurately calculate the formation energies of charged defects. The most general scheme is the *bulk* VBM method, corrected by the difference of average effective potentials. However, this correction has a small effect on the formation energies of simple defects in diamond, and the ionization levels are in good overall agreement with the exact values when the *defect* VBM is used.

ACKNOWLEDGMENTS

This work has been supported by a grant from the Korean Research Foundation (2002-070-C00048) and the Academy of Finland through the Center of Excellence Program (2002-2005). The authors gratefully acknowledge the generous provision of computing resources by the Center for Scientific Computing (CSC), Espoo, Finland.

[1] J. Isoya, H. Kanda, Y. Uchida, S. C. Lawson, S. Yamasaki, H. Itoh, and Y. Morita, Phys. Rev. B **45**, 1436 (1992).

[2] G. Davies, S. C. Lawson, A. T. Collins, A. Mainwood, and S. J. Sharp, Phys. Rev. B **46**, 13 157 (1992).

[3] J. A. van Wyk, O. D. Tucker, M. E. Newton, J. M. Baker, G. S. Woods, and P. Spear, Phys. Rev. B **52**, 12 657 (1995).

[4] J. A. Garrido, C. E. Nebel, M. Stutzmann, E. Gheeraer, N. Casanova, E. Bustarret, and A. Deneuville, Diamond Relat.

Mater. **11**, 347 (2002).
[5] J. A. Garrido, C. E. Nebel, M. Stutzmann, E. Gheeraert, N. Casanova, and E. Bustarret, Phys. Rev. B **65**, 165409 (2002).
[6] A. Pu, V. Avalos, and S. Dannefaer, Diamond Relat. Mater. **10**, 585 (2001).
[7] S. Dannefaer, A. Pu, and D. Kerr, Diamond Relat. Mater. **10**, 2113 (2001).
[8] C. E. Nebel, R. Zeisel, and M. Stutzmann, Phys. Status Solidi A **174**, 117 (1999).
[9] M. Bruzzi, D. Menichelli, S. Pirollo, and S. Sciortino, Diamond Relat. Mater. **9**, 1081 (2000).
[10] M. Pesola, Y. J. Lee, J. von Boehm, M. Kaukonen, and R. M. Nieminen, Phys. Rev. Lett. **84** 5343 (2000).
[11] C. H. Park and D. J. Chadi, Phys. Rev. Lett. **82**, 113 (1999).
[12] D. J. Chadi, Phys. Rev. B **68**, 193204 (2003).
[13] S. B. Zhang and J. E. Northrup, Phys. Rev. Lett. **67**, 2339 (1991).
[14] J. Bernholc, A. Antonelli, T. M. Del Sole, Y. Bar-Yam, and S. T. Pantelides, Phys. Rev. Lett. **61**, 2689 (1988).
[15] Y. J. Lee, J. von Boehm, M. Pesola, and R. M. Nieminen, Phys. Rev. Lett. **86** 3060 (2001).
[16] Y. J. Lee, J. von Boehm, M. Pesola, and R. M. Nieminen, Phys. Rev. B **65** 085205 (2002).
[17] S. Wang, M. Di Ventra, S. G. Kim, and S. T. Pantelides, Phys. Rev. Lett. **86** 5946 (2001).
[18] M. J. Puska, S. Pöykkö, M. Pesola, and R. M. Nieminen, Phys. Rev. B **58**, 1318 (1998).
[19] S. Ögüt, H. Kim, and J. R. Chelikowsky, Phys. Rev. B **56**, R11 353 (1997).
[20] O. Sugino and A. Oshiyama, Phys. Rev. Lett. **68**, 1858 (1992).
[21] L. Torpo, M. Marlo, T. E. M. Staab, and R. M. Nieminen, J. Phys.: Condens. Matter **13**, 6203 (2001).
[22] P. Boguslawski, E. L. Briggs, and J. Bernholc, Phys. Rev. B **51**, 17 255 (1995).
[23] S. J. Breuer and P. R. Briddon, Phys. Rev. B **51**, 6984 (1995).
[24] A. Zywietz, J. Furthmüller, and F. Bechstedt, Phys. Status Solidi A **210**, 13 (1998).
[25] J. E. Northrup and S. B. Zhang, Phys. Rev. B **47**, 6791 (1993).
[26] S. W. de Leeuw, J. W. Perram, and E. R. Smith, Proc. R. Soc. London, Ser. A **373**, 27 (1980).
[27] M. Leslie and M. J. Gillan, J. Phys. C **18**, 973 (1985).
[28] G. Makov and M. C. Payne, Phys. Rev. B **51**, 4014 (1995).
[29] M. R. Jarvis, I. D. White, R. W. Godby, and M. C. Payne, Phys. Rev. B **56**, 14 972 (1997).
[30] L. N. Kantorovich, Phys. Rev. B **60**, 15 476 (1999).
[31] J. Lento, J.-L. Mozos, and R. M. Nieminen, J. Phys.: Condens. Matter **14**, 2637 (2002).
[32] L. Torpo, T. E. M. Staab, and R. M. Nieminen, Phys. Rev. B **65**, 085202 (2002).
[33] D. Segev and S. H. Wei, Phys. Rev. Lett. **91**, 126406 (2003).
[34] U. Gerstmann, P. Deák, R. Rurali, B. Aradi, Th. Frauenheim, and H. Overhof, Physica B **340**, 190 (2003).
[35] P. A. Schultz, Phys. Rev. B **60**, 1551 (1999).
[36] P. A. Schultz, Phys. Rev. Lett. **84**, 1942 (2000).
[37] A. Garcia and J. E. Northrup, Phys. Rev. Lett. **74**, 1131 (1995).
[38] A. Zywietz, J. Furthmüller, and F. Bechstedt, Phys. Rev. B **59**, 15 166 (1999).
[39] A. Resende, R. Jones, S. Öberg, and P. R. Briddon, Phys. Rev. Lett. **82**, 2111 (1999).
[40] J.-W. Jeong and A. Oshiyama, Phys. Rev. B **64**, 235204 (2001).
[41] J. Coutinho, V. J. B. Torres, R. Jones, and P. R. Briddon, Phys. Rev. B **67**, 035205 (2003).
[42] J. P. Perdew, K. Burke, and M. Ernzerhof, Phys. Rev. Lett. **77**, 3865 (1996).
[43] P. Ordejón, E. Artacho, and J. M. Soler, Phys. Rev. B **53**, R10 441 (1996).
[44] The total net charge must equal zero for the entire supercell to satisfy charge neutrality. The volume of the 216-atom supercell is equivalent to a sphere of $r=6.8$ Å; it is observed that $Q(r)$ equals zero at around $r=6.8$ Å for all the cases presented.
[45] J. Shim, Y. J. Lee, R. M. Nieminen, and E.-K. Lee (unpublished).